International Journal for
NUMERICAL METHODS IN
FLUIDS

A conservative semi-implicit method for coupled surface-subsurface flows in regional scale

Journal:	*International Journal for Numerical Methods in Fluids*
Manuscript ID:	Draft
Wiley - Manuscript type:	Research Article
Date Submitted by the Author:	n/a
Complete List of Authors:	Casulli, Vincenzo; University of Trento, Civil and Environmental Engineering;
Keywords:	free-surface flow, semi-implicit method, subgrid resolution, mildly nonlinear system, surface-subsurface flow, pressurized flow

INTERNATIONAL JOURNAL FOR NUMERICAL METHODS IN FLUIDS

Int. J. Numer. Meth. Fluids 2015; **00**:1–25

Published online in Wiley InterScience (www.interscience.wiley.com). DOI: 10.1002/fld

A conservative semi-implicit method for coupled surface-subsurface flows in regional scale

Vincenzo Casulli *

Laboratory of Applied Mathematics, Department of Civil, Environmental and Mechanical Engineering, University of Trento, Via Mesiano, 77 – I-38123 Trento, Italy

SUMMARY

A semi-implicit method for coupled surface-subsurface flows in regional scale is proposed and analyzed. The flow domain is assumed to have a small vertical scale as compared to the horizontal extents. Thus, after hydrostatic approximation, the simplified governing equations are derived from the Reynolds averaged Navier-Stokes equations for the surface flow, and from the Darcy's law for the sub-surface flow. A conservative free-surface equation is derived from a vertical integral of the incompressibility condition and extends to the whole water column including both, the surface and the subsurface wet domain. Numerically, the horizontal domain is covered by an unstructured orthogonal grid that may include subgrid specifications. Along the vertical direction a simple z-layer discretization is adopted. Semi-implicit finite difference equations for velocities, and a finite volume approximation for the free-surface equation, are derived in such a fashion that, after simple manipulation, the resulting discrete free-surface equation yields a single, well posed, mildly nonlinear system. This system is efficiently solved by a nested Newton type iterative method which yields simultaneously the pressure and a nonnegative fluid volume throughout the computational grid. The time step size is not restricted by stability conditions dictated by friction or surface wave speed. The resulting algorithm is simple, extremely efficient and very accurate. Exact mass conservation is assured also in presence of wetting and drying dynamics, in pressurized flow conditions, and during free-surface transition through the interface. A few examples illustrate the model applicability and demonstrate the effectiveness of the proposed algorithm. Copyright © 2015 John Wiley & Sons, Ltd.

Received . . .

KEY WORDS: free-surface flow; semi-implicit method; subgrid resolution; mildly nonlinear system; surface-subsurface flow; pressurized flow

1. INTRODUCTION

Numerical modelling of coupled surface-subsurface flows is an interesting task that has received considerable attention for several decades. Preliminarily, one has to choose an appropriate set of governing differential equations whose validity needs to be established in both, the surface and in the subsurface flow domain. For surface flows the choice may range from an oversimplified diffusion approximation of the Saint Venant equations to the full three-dimensional Navier-Stokes equations

*Correspondence to: vincenzo.casulli@unitn.it

with complex free-surfaces. For the sub-surface dynamic, the choice of a differential model may range from the Boussinesq equation to the three-dimensional Richards equation that includes non-hydrostatic pressure and variably unsaturated flows [1].

Numerically, surface and subsurface flows have often received separate attention and in most cases impressive results have been produced and reported. Several attempts have been made to couple surface and subsurface numerical models with different coupling strategies (see, e.g., [2, 3, 4, 5] and the numerous references therein). The simplest (non-iterative) strategy consists in applying sequentially, within each time step, the surface flow model and the subsurface model. The accuracy of this approach can be improved by adopting an iterative coupling having the objective to better approximate the boundary conditions at the interface between the surface and the subsurface region. The higher computational effort required by an iterative approach may be compensated by the better accuracy so achieved, but a rigorous convergence analysis of an iterative approach may be difficult to establish [6] and mass conservation is often inaccurate especially in presence of wetting and drying dynamics, in pressurized flow conditions, in inhomogeneous porous medium, and during free-surface transition through the interface.

The spatial domain of environmental flows in regional scale is typically characterized by having a much larger horizontal extent than the vertical one. These flows are prevalently horizontal and the hydrostatic approximation (also known as Dupuit's assumption) is assumed to be valid throughout [1]. One further assumes that the flow is confined below by an impervious bedrock, and above by a free-surface (phreatic surface or water table) which may intersect an impermeable ceiling, in which case below the ceiling the flow is said to be pressurized. With these assumptions the pressure can be conveniently expressed in terms of the free-surface elevation (or piezometric head) and the two flows, namely the surface flow and the subsurface flow, share the same (hydrostatic) pressure.

In the present investigation a *conservative* form of the free-surface equation is derived in such a fashion that the time rate of the water level is expressed in terms of the total balance over the entire water column and includes both, the surface and the subsurface horizontal fluxes. The resulting free-surface equation incorporates the normal velocity boundary condition at the impervious bottom, the

Prepared using fldauth.cls http://mc.manuscriptcentral.com/fluids DOI: 10.1002/fld

kinematic boundary condition at the free surface and the normal flow continuity at the interface between the surface and the subsurface flow region.

Numerically, semi-implicit methods are known to be stable at a minimal computational cost [7, 8, 9, 10]. Additionally, when subgrid geometrical details are properly incorporated into a numerical model for surface flows, then significant improvements of numerical accuracy may be achieved on relatively coarse computational grids [11, 12, 13]. Similarly, efficient and highly accurate numerical methods for subsurface flows can be derived by using semi-implicit approximations that incorporate subgrid geometrical details [14, 15, 16]. Here, these methods are generalized to form a single semi-implicit algorithm that applies to coupled surface-subsurface flows, and simplifies to either a surface or a subsurface model as particular cases.

Specifically, only the velocities in the free-surface equation, and the pressure gradient, the vertical viscosity and the friction in the discrete velocity equations are approximated at the new time level. Next, a formal substitution of the unknown velocities into the discrete free-surface equation leads to a reduced mildly non linear system where the new free-surface elevations are the only unknowns. This system is iteratively solved by a properly devised converging method [14, 15] which yields, *simultaneously*, the new free-surface location and the corresponding nonnegative fluid volume on each water column of the horizontal computational grid. Once the new free surface (hence the pressure) is known, the horizontal velocities are readily computed from the discrete velocity equations. Finally, the new vertical component of the velocity is recovered recursively from a finite volume approximation of the incompressibility condition.

The resulting algorithm is relatively simple, extremely accurate, and numerically stable. Moreover, exact mass conservation is assured throughout also in presence of wetting and drying and during the free-surface transition from surface to the subsurface region or viceversa.

The remainder of this paper is organized as follows: the governing differential equations are first introduced and discussed in Section 2. In Section 3 the discrete flow variables are defined on a staggered computational grid that may include subgrid specifications. Then, a non linear semi-implicit method is derived in Section 4. In Section 5 a practical solution algorithm is provided.

Prepared using fldauth.cls http://mc.manuscriptcentral.com/fluids DOI: 10.1002/fld

Several hints and remarks are outlined in Section 6 and, finally, in Section 7 this method is applied to some illustrative examples of different surface-subsurface flow problems.

2. THE GOVERNING DIFFERENTIAL EQUATIONS

For the sake of simplicity, the three-dimensional free-surface flow of an incompressible fluid is considered to be bounded by an impervious bedrock located at $z = -h(x, y)$ and by an impermeable ceiling located at $z = c(x, y) \geq -h(x, y)$. Both $h(x, y)$ and $c(x, y)$ are assumed to be known for all $(x, y) \in \Omega$ where Ω denotes the horizontal extent of the region being investigated. Additionally, the surface and the sub-surface flow regions are separated at $z = -s(x, y)$ where the soil level $s(x, y)$ is prescribed for all $(x, y) \in \Omega$ and satisfies $-h(x, y) \leq -s(x, y) \leq c(x, y)$. The porous material is characterized by a porosity $\epsilon(x, y, z)$ and hydraulic conductivity $\mathcal{K}(x, y, z)$ that are prescribed for all $(x, y) \in \Omega$ and for all $z \in [-h(x), -s(x)]$. For notational convenience the porosity function is prolonged as $\epsilon(x, y, z) = 1$ for all $z \in [-s(x, y), c(x, y)]$ and $\epsilon(x, y, z) = 0$ for all $z \notin [-h(x, y), c(x, y)]$.

Note that if $s(x, y) = h(x, y)$ for all $(x, y) \in \Omega$, then the subsurface region is being neglected and only surface flow is allowed. Likewise, if $s(x, y) = -c(x, y)$ for all $(x, y) \in \Omega$, then the surface region is being neglected and only subsurface flow is permitted.

2.1. *Governing equations for surface flows*

Within a Cartesian coordinate system (x, y, z) where the x, y-axis are horizontal and the vertical z-axis is oriented upward along the gravity direction, the horizontal momentum equations for surface flows are given by

$$\frac{\partial u}{\partial t} + u\frac{\partial u}{\partial x} + v\frac{\partial u}{\partial y} + w\frac{\partial u}{\partial z} = -g\frac{\partial \eta}{\partial x} + \frac{\partial}{\partial x}\left(\nu^h \frac{\partial u}{\partial x}\right) + \frac{\partial}{\partial y}\left(\nu^h \frac{\partial u}{\partial y}\right) + \frac{\partial}{\partial z}\left(\nu^v \frac{\partial u}{\partial z}\right) \quad (1)$$

$$\frac{\partial v}{\partial t} + u\frac{\partial v}{\partial x} + v\frac{\partial v}{\partial y} + w\frac{\partial v}{\partial z} = -g\frac{\partial \eta}{\partial y} + \frac{\partial}{\partial x}\left(\nu^h \frac{\partial v}{\partial x}\right) + \frac{\partial}{\partial y}\left(\nu^h \frac{\partial v}{\partial y}\right) + \frac{\partial}{\partial z}\left(\nu^v \frac{\partial v}{\partial z}\right) \quad (2)$$

Prepared using fldauth.cls http://mc.manuscriptcentral.com/fluids DOI: 10.1002/fld

where $u(x,y,z,t)$, $v(x,y,z,t)$ and $w(x,y,z,t)$ are the unknown velocity components in the horizontal x-, y- and in the vertical z-directions, respectively; t is the time; g is the gravitational acceleration; $\eta(x,y,t)$ is the free-surface elevation; and ν^h and ν^v are prescribed non-negative coefficients of horizontal and vertical viscosity, respectively.

Without loss of generality, the wind friction is neglected so that the boundary conditions at the free-surface and at the solid walls are assumed to be

$$\left.\begin{array}{ll} \nu^v \frac{\partial u}{\partial z} = 0 & \\ & \text{at } z=\eta, \\ \nu^v \frac{\partial v}{\partial z} = 0 & \end{array}\right\} \qquad \left.\begin{array}{ll} \nu^v \frac{\partial u}{\partial z} = \gamma u^* & \\ & \text{at } z=-s \text{ and } z=c \\ \nu^v \frac{\partial v}{\partial z} = \gamma v^* & \end{array}\right\} \tag{3}$$

where $\gamma(x,y,t)$ is a nonnegative bottom friction coefficient and u^* and v^* are the horizontal velocity components near the solid boundary.

The differential Equations (1)–(2) are the model equations that describe the surface flow within a time dependent three-dimensional domain which is identified by $(x,y) \in \Omega$ and $s(x,y) + min[\eta(x,y,t), c(x,y)] > 0$.

At the initial time $t=0$ the velocities $u(x,y,z,0)$, $v(x,y,z,0)$ and $w(x,y,z,0)$ are prescribed as initial conditions. The initial fluid position is specified by prescribing $\eta(x,y,0)$ for all $(x,y) \in \Omega$.

2.2. *Governing equations for sub-surface flows*

The horizontal velocities in the sub-surface region are given by

$$u = -\mathcal{K}\frac{\partial \eta}{\partial x} \tag{4}$$

$$v = -\mathcal{K}\frac{\partial \eta}{\partial y} \tag{5}$$

where $\mathcal{K}(x,y,z)$ is the nonnegative hydraulic conductivity.

The differential Equations (4)–(5) are the model equations that describe the subsurface flow within a time dependent three-dimensional domain which is identified by $(x,y) \in \Omega$ and $h(x,y) + min[\eta(x,y,t), c(x,y), -s(x,y)] > 0$.

DOI: 10.1002/fld

Note that at any point $(x, y) \in \Omega$, if $-s(x, y) < \eta(x, y, t) < c(x, y)$, then the unknown function $\eta(x, y, t)$ represents the free-surface elevation. If $\eta(x, y, t) \leq -s(x, y)$ then the surface layer is dry, Equations (1)–(2) do not apply at (x, y), and $\eta(x, y, t)$ represents the phreatic surface or water table of the subsurface wet region. Finally, if $\eta(x, y, t) \geq c(x, y)$ then (x, y) is pressurized and $\eta(x, y, t)$ represents the piezometric head. In all cases the unknown function $\eta(x, y, t)$ in Equations (1)–(2) and (4)–(5) represents the local (hydrostatic) pressure.

2.3. *Free-surface and interface condition*

At the common interface between surface and subsurface regions continuity of mass transfer is assumed. Moreover, fluid incompressibility in both regions is assured by the following incompressibility condition

$$\frac{\partial u}{\partial x} + \frac{\partial v}{\partial y} + \frac{\partial w}{\partial z} = 0 \tag{6}$$

By using the Leibniz integral rule and the kinematic boundary conditions at the impervious bottom and at the free-surface, integration of the continuity equation (6) over the depth yields the following free-surface equation in conservative form

$$\frac{\partial}{\partial t}\left(\int_{-h}^{\eta} \epsilon \, dz\right) + \frac{\partial}{\partial x}\left(\int_{-h}^{\eta} u \, dz\right) + \frac{\partial}{\partial y}\left(\int_{-h}^{\eta} v \, dz\right) = 0 \tag{7}$$

Equation (7) is the vertically integrated continuity equation expressing a mass balance over the entire water column for all $(x, y) \in \Omega$ and for all $t > 0$. Note that this equation includes both, the surface and the subsurface horizontal fluxes. In addition to the normal velocity boundary condition at the impervious bottom, and the kinematic boundary condition at the free surface, Equation (7) also incorporates the normal flow continuity at the interface between the surface and the subsurface flow region.

Prepared using fldauth.cls http://mc.manuscriptcentral.com/fluids DOI: 10.1002/fld

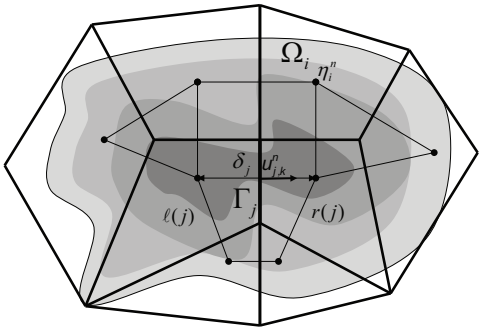

Figure 1. Discrete flow variables on a staggered orthogonal grid

3. UNSTRUCTURED GRID AND SUBGRID

In order to solve equations (1)–(7) numerically, the region Ω is covered by an *unstructured orthogonal grid* [10] consisting of a set of non-overlapping convex polygons $\Omega_i,\ i = 1, 2, ..., N_p$ separated by N_s sides $\Gamma_j,\ j = 1, 2, \ldots, N_s$. Within each polygon a *center* must be identified in such a way that the segment joining the centers of two adjacent polygons and the side shared by the two polygons, have a non empty intersection and are *orthogonal* to each other (see Figure 1).

Once Ω has been covered with an unstructured orthogonal grid, each polygon Ω_i may have an arbitrary number of sides. Let S_i denote the set of sides of the ith polygon. The left and the right polygons which share the jth internal side are identified by the indices $\ell(j)$ and $r(j)$, respectively. Moreover, $\wp(i, j)$ denotes the neighbor of polygon i that shares side j with the ith polygon. The nonzero distance between the centers of two adjacent polygons which share the jth internal side is denoted with δ_j and the length of each side is denoted by $\lambda_j,\ j = 1, 2, ..., N_s$.

Along the vertical direction a simple finite difference discretization, not necessarily uniform, is adopted. By denoting with $z_{k+\frac{1}{2}}$ a given level surface, the vertical discretization step is defined by $\Delta z_k = z_{k+\frac{1}{2}} - z_{k-\frac{1}{2}},\ k = 1, 2, \ldots, N_z$.

The three-dimensional space discretization consists of *bathymetry shaved* volumes contained in prisms whose horizontal faces are the polygons at two consecutive level surfaces, and whose height is Δz_k. The discrete water surface elevation η_i^n at time level t_n, assumed to be constant within each polygon, is located at the center of the ith polygon.

DOI: 10.1002/fld

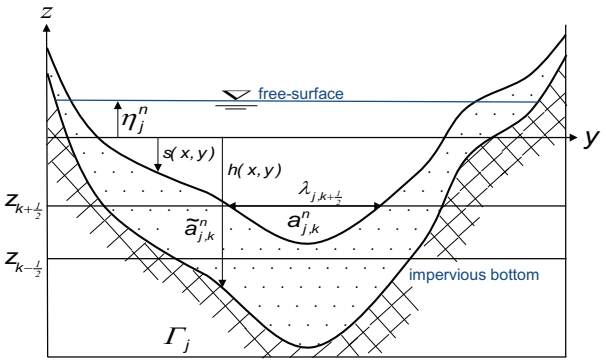

Figure 2. Vertical cross section along edge Γ_j

For any prescribed water level $\eta_i^n,\ i = 1, 2, \ldots, N_p$, a value for η_j^n along each internal edge Γ_j is derived from the nearest grid values by taking, e.g., the average, the upwind or the maximum between $\eta_{\ell(j)}^n$ and $\eta_{r(j)}^n$ (see Figure 2).

The wet length of the jth edge at $z_{k+\frac{1}{2}}$ is given by

$$\lambda_{j,k+\frac{1}{2}}^n = \int_{\Gamma_j} \mathcal{H}\left(min(\eta_j^n, c) - z_{k+\frac{1}{2}}\right) \mathcal{H}\left(z_{k+\frac{1}{2}} + s\right) d\Gamma \tag{8}$$

where $\mathcal{H}$ is the Heaviside step function which is *one* when its argument is strictly positive and *zero* otherwise. Note that $0 \le \lambda_{j,k+\frac{1}{2}}^n \le \lambda_j$.

The nonnegative *surface wet area* of each vertical face of the computational grid is taken to be

$$\bar{a}_{j,k}^n = \int_{\Gamma_j} \Delta\bar{z}_{j,k}^n d\Gamma \tag{9}$$

where $\Delta\bar{z}_{j,k}^n$ is the *surface wetted distance* between $z_{k+\frac{1}{2}}$ and $z_{k-\frac{1}{2}}$ along Γ_j. Specifically, $\Delta\bar{z}_{j,k}^n$ is given by $\Delta\bar{z}_{j,k}^n = max[0, min(z_{k+\frac{1}{2}}, \eta_j^n, c) - max(z_{k-\frac{1}{2}}, -s)]$. Note that $0 \le \bar{a}_{j,k}^n \le \lambda_j \Delta z_k$.

Likewise, the nonnegative *subsurface wet area* of each vertical face of the computational grid is taken to be

$$\tilde{a}_{j,k}^n = \int_{\Gamma_j} \Delta\tilde{z}_{j,k}^n d\Gamma \tag{10}$$

where $\Delta\tilde{z}_{j,k}^n$ is the *subsurface wetted distance* between $z_{k+\frac{1}{2}}$ and $z_{k-\frac{1}{2}}$ along Γ_j. Specifically, $\Delta\tilde{z}_{j,k}^n$ is given by $\Delta\tilde{z}_{j,k}^n = max[0, min(z_{k+\frac{1}{2}}, \eta_j^n, -s) - max(z_{k-\frac{1}{2}}, -h)]$. Note that $0 \le \tilde{a}_{j,k}^n \le \lambda_j \Delta z_k$.

Prepared using fldauth.cls http://mc.manuscriptcentral.com/fluids DOI: 10.1002/fld

Moreover, by denoting with $a^n_{j,k}$ the total face wet area, namely $a^n_{j,k} = \bar{a}^n_{j,k} + \tilde{a}^n_{j,k}$, one has $0 \leq a^n_{j,k} \leq \lambda_j \Delta z_k$

The horizontal surface and subsurface velocities perpendicular to each wet vertical face of the computational grid, assumed to be constants over the face, are denoted with $\bar{u}^n_{j,k}$ and $\tilde{u}^n_{j,k}$, respectively. Additionally, if the total face wet area is at least partially wet ($a^n_{j,k} > 0$), then the corresponding face average horizontal velocity is given by

$$u^n_{j,k} = \frac{\bar{u}^n_{j,k}\bar{a}^n_{j,k} + \tilde{u}^n_{j,k}\tilde{a}^n_{j,k}}{a^n_{j,k}} \tag{11}$$

The positive direction for $u^n_{j,k}$, $\bar{u}^n_{j,k}$ and $\tilde{u}^n_{j,k}$ is chosen to go from $\ell(j)$ to $r(j)$.

The face average (surface and subsurface) vertical velocity is defined on each horizontal wet face of the computational grid and is denoted by $w^n_{i,k+\frac{1}{2}}$. The corresponding total wet area is given by

$$a^n_{i,k+\frac{1}{2}} = \int_{\Omega_i} \mathcal{H}\left(min(\eta^n_i, c) - z_{k+\frac{1}{2}}\right) \mathcal{H}\left(z_{k+\frac{1}{2}} + h\right) d\Omega \tag{12}$$

and satisfies $0 \leq a^n_{i,k+\frac{1}{2}} \leq P_i$.

4. FINITE DIFFERENCE – FINITE VOLUME APPROXIMATION

Equations (1)–(7) will be discretized on an unstructured orthogonal grid by using a finite difference approximation for the velocity Equations (1)–(5) and a finite volume approximation for the continuity Equations (6)–(7).

4.1. Finite difference approximation for surface horizontal velocities

With a semi-implicit method the terms to be discretized at the new time level are carefully selected as to obtain a stable method with a minimal computational effort [7, 8, 9, 10]. Thus, the advective and the viscous terms of the momentum equations are discretized explicitly, whereas the pressure gradient in the momentum equations, and the velocities in the free-surface equation (7) are discretized implicitly. Moreover, the vertical viscosity and the wall friction terms are taken implicitly. Thus, since Equations (1)–(2) are invariant under solid rotation of the x and y axis on

Prepared using fldauth.cls http://mc.manuscriptcentral.com/fluids DOI: 10.1002/fld

the horizontal plane, a consistent semi-implicit *finite-difference* discretization for the momentum Equations (1)–(2) on each edge Γ_j is taken to be

$$\begin{aligned}\bar{a}^n_{j,k}\bar{u}^{n+1}_{j,k} &= \bar{a}^n_{j,k}F\bar{u}^n_{j,k} - g\Delta t\bar{a}^n_{j,k}\frac{\eta^{n+\theta}_{r(j)} - \eta^{n+\theta}_{\ell(j)}}{\delta_j} - \Delta t\gamma^n_{j,k}\bar{u}^{n+1}_{j,k} \\ &+ \Delta t\left\{\lambda^n_{j,k+\frac{1}{2}}\nu^v_{j,k+\frac{1}{2}}\frac{\bar{u}^{n+1}_{j,k+1} - \bar{u}^{n+1}_{j,k}}{\Delta z_{k+\frac{1}{2}}} - \lambda^n_{j,k-\frac{1}{2}}\nu^v_{j,k-\frac{1}{2}}\frac{\bar{u}^{n+1}_{j,k} - \bar{u}^{n+1}_{j,k-1}}{\Delta z_{k-\frac{1}{2}}}\right\}\end{aligned}$$

$$k = \bar{m}_j, \bar{m}_j + 1, \ldots, \bar{M}^n_j \qquad (13)$$

where F is any stable non-linear difference operator that includes a spatial discretization of the advective and horizontal viscous terms; Δt is the time step size; $\eta^{n+\theta} = \theta\eta^{n+1} + (1-\theta)\eta^n$ and $\theta \in [\frac{1}{2}, 1]$ is an implicitness parameter; $\gamma^n_{j,k}$ is a nonnegative wall friction coefficient which accounts for the boundary conditions (3) and is proportional to the wetted perimeter of the (j,k)th vertical face at solid walls; and $\bar{m}_j$ and $\bar{M}^n_j$ denote the lowest and the highest surface wet vertical face, respectively. As indicated $\bar{m}_j$ and $\bar{M}^n_j$ depend on their spatial location j and $\bar{M}^n_j$ may also change with the time level t_n in order to account for the free-surface dynamics. Clearly, $\bar{a}^n_{j,k} > 0$ for all $k = \bar{m}_j, \bar{m}_j + 1, \ldots, \bar{M}^n_j$; moreover $\lambda^n_{j,k+\frac{1}{2}} > 0$ for all $k = \bar{m}_j, \bar{m}_j + 1, \ldots, \bar{M}^n_j - 1$, and $\lambda^n_{j,\bar{m}-\frac{1}{2}} = \lambda^n_{j,\bar{M}+\frac{1}{2}} = 0$.

A particular form for F in Equation (13) can be chosen in a variety of ways, such as by using an Eulerian-Lagrangian scheme [7, 8, 9, 10], or an explicit conservative formulation [17]. Since this topic is widely covered in the literature, a specific formulation for obtaining $F\bar{u}^n_{j,k}$ will not be elaborated in the present study. Here, we only insist that F be a *stable* operator in the sense that if F is only conditionally stable, then that stability condition will be the stability condition required by the method being developed.

Of course, Equation (13) is defined only on wet vertical faces, *i.e.*, where $\bar{a}^n_{j,k} > 0$. On dry faces $\bar{u}^{n+1}_{j,k} = 0$ is assumed. Thus, for any structure given to F, one has exactly one linear equation (13) for each unknown surface velocity $\bar{u}^{n+1}_{j,k}$.

Prepared using fldauth.cls http://mc.manuscriptcentral.com/fluids DOI: 10.1002/fld

4.2. *Finite difference approximation for subsurface horizontal velocities*

The Darcy's Equations (4)–(5) do not contain time derivatives, thus they must be satisfied at each time level. These equations are invariant under solid rotation of the x and y axis on the horizontal plane. Hence, within the subsurface flow region, and with a properly oriented coordinate system, a simple implicit finite difference approximation for Equations (4)–(5) is taken to be

$$\tilde{u}_{j,k}^{n+1} = -\mathcal{K}_{j,k}\frac{\eta_{r(j)}^{n+1} - \eta_{\ell(j)}^{n+1}}{\delta_j}, \qquad k = \tilde{m}_j, \tilde{m}_j + 1, \ldots, \tilde{M}_j^n \tag{14}$$

where $\mathcal{K}_{j,k}$ is the face averaged hydraulic conductivity; and $\tilde{m}_j$ and $\tilde{M}_j^n$ denote the lowest and the highest subsurface wet vertical face, respectively. As indicated $\tilde{m}_j$ and $\tilde{M}_j^n$ depend on their spatial location j and $\tilde{M}_j^n$ may also change with the time level t_n in order to account for the free-surface dynamics. Clearly, $\tilde{a}_{j,k}^n > 0$ for all $k = \tilde{m}_j, \tilde{m}_j + 1, \ldots, \tilde{M}_j^n$.

Of course, Equation (14) is defined only on wet vertical faces, *i.e.*, where $\tilde{a}_{j,k}^n > 0$. On dry faces $\tilde{u}_{j,k}^{n+1} = 0$ is assumed. Thus, for each unknown subsurface velocity $\tilde{u}_{j,k}^{n+1}$, one has exactly one linear equation (14).

4.3. *Finite volume approximation for the incompressibility condition*

The continuity Equation (6) is approximated at the new time level t_{n+1} in such a fashion that the resulting face averaged velocity field is discrete divergence-free in every control volume below the free-surface. Indeed, a volume integral of Equation (6) yields a consistent *finite volume* form of the incompressibility condition (6) which is given by

$$\left(\sum_{j\in S_i} \sigma_{i,j} a_{j,k}^n u_{j,k}^{n+1}\right) + a_{i,k+\frac{1}{2}}^n w_{i,k+\frac{1}{2}}^{n+1} - a_{i,k-\frac{1}{2}}^n w_{i,k-\frac{1}{2}}^{n+1} = 0 \tag{15}$$

where $a_{j,k}^n$ and $a_{i,k\pm\frac{1}{2}}^n$ are the total wet areas; $u_{j,k}^{n+1}$ and $w_{i,k\pm\frac{1}{2}}^{n+1}$ are the corresponding new face averaged velocities; and $\sigma_{i,j}$ is a sign function associated with the orientation of the normal velocities defined on the jth vertical faces. Specifically,

Prepared using fldauth.cls http://mc.manuscriptcentral.com/fluids DOI: 10.1002/fld

$$\sigma_{i,j} = \frac{r(j) - 2i + \ell(j)}{r(j) - \ell(j)}$$

The vertical k index in Equation (15) ranges from m_i to $M_i^n - 1$, where m_i and M_i^n denote the lowest and the highest control volume within the ith water column. Incompressibility in the top (M_i^nth) control volume has to account for the free-surface dynamic and will result from a conservative approximation of the free-surface equation (7). Thus, one has exactly one linear equation (15) for each unknown vertical velocity $w_{i,k+\frac{1}{2}}^{n+1},\ k = m_i, m_i+1, \ldots, M_i^n - 1$.

4.4. Finite volume approximation for the free-surface equation

Finally, in order to close the system, a consistent discretization of the free-surface Equation (7) in flux form is obtained upon integration of Equation (7) over the ith polygon. This yields the following semi-implicit *finite volume* approximation

$$V_i(\eta_i^{n+1}) = V_i(\eta_i^n) - \Delta t \sum_{j \in S_i} \sigma_{i,j} \left(\sum_{k=\bar{m}_j}^{\bar{M}_j^n} \bar{a}_{j,k}^n \bar{u}_{j,k}^{n+\theta} + \sum_{k=\tilde{m}_j}^{\tilde{M}_j^n} \tilde{a}_{j,k}^n \tilde{u}_{j,k}^{n+\theta} \right) \tag{16}$$

where $\bar{u}_{j,k}^{n+\theta} = \theta \bar{u}_{j,k}^{n+1} + (1-\theta)\bar{u}_{j,k}^n$; $\tilde{u}_{j,k}^{n+\theta} = \theta \tilde{u}_{j,k}^{n+1} + (1-\theta)\tilde{u}_{j,k}^n$; and

$$V_i(\eta_i^{n+1}) = \int_{\Omega_i} \left[\int_{-\infty}^{\eta_i^{n+1}} \epsilon(x,y,z) dz \right] dx\, dy \tag{17}$$

is the water volume within the ith water column for the specified water level η_i^{n+1}, for any porosity distribution ϵ, and for any prescribed geometric detail h, s and c.

Equation (16) applies to each water column identified by the corresponding polygon Ω_i. Thus, one has exactly one equation (16) for each unknown water level $\eta_i^{n+1},\ i = 1, 2, \ldots, N_p$. Moreover, equation (16) expresses an exact mass balance for every water column regardless of the free-surface locations η_i^n and η_i^{n+1}. This equation, however, is *mildly nonlinear* and the nonlinearity resides in the definition of the fluid volume $V_i(\eta_i^{n+1})$ at the left hand side of Equation (16). Note that if the fluid volume $V_i(\eta_i^{n+1})$ is linearized as $V_i(\eta_i^{n+1}) = V_i(\eta_i^n) + V_i'(\eta_i^n)(\eta_i^{n+1} - \eta_i^n)$, then Equation (16) becomes linear but mass conservation can *no longer* be guaranteed.

Prepared using fldauth.cls http://mc.manuscriptcentral.com/fluids DOI: 10.1002/fld

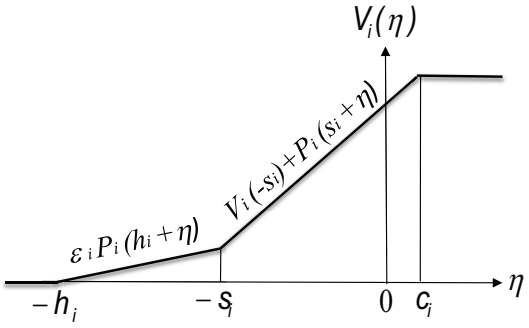

Figure 3. Graphical representation of a simple piecewise linear volume function

Figure 3 illustrates the volume variability in the very simple case of constants $h(x, y) = h_i$, $s(x, y) = s_i$ and $c(x, y) = c_i$ for all $(x, y) \in \Omega_i$, and constant porosity distribution $\epsilon(x, y, z) = \epsilon_i$ for all $(x, y) \in \Omega_i$ and for all $z \in [-h_i, -s_i]$. In this case the i-th fluid volume remains zero for all $\eta \leq -h_i$, it grows linearly with slope $\epsilon_i P_i$ when $-h_i \leq \eta \leq -s_i$, it grows with a steeper slope P_i when $-s_i \leq \eta \leq c_i$, and finally remains constant $V_i(\eta) = P_i[\epsilon_i(h_i - s_i) + s_i + c_i]$ when the ith water column is pressurized, that is for all $\eta \geq c_i$. In all cases the fluid volume $V_i(\eta_i^{n+1})$ is always a nonnegative and non decreasing function of η_i^{n+1}.

All together, Equations (13), (14), (15) and (16) constitute a mildly nonlinear system of at most $N_z(2N_s + N_p)$ equations. This system has to be solved at each time step in order to determine the new field variables $\bar{u}_{j,k}^{n+1}$, $\tilde{u}_{j,k}^{n+1}$, $w_{i,k+\frac{1}{2}}^{n+1}$ and η_i^{n+1} throughout the computational grid.

5. SOLUTION ALGORITHM

The system of $N_z(2N_s + N_p)$ equations formed by (13)-(16) can be conveniently decomposed into a reduced *mildly nonlinear* system of N_p equations for η_i^{n+1}; a set of N_s independent linear tridiagonal systems of at most N_z equations for the surface horizontal velocities $\bar{u}_{j,k}^{n+1}$; $N_s N_z$ explicit equations for the subsurface horizontal velocities $\tilde{u}_{j,k}^{n+1}$; and a set of N_p independent recursive formulas to derive the new vertical velocity $w_{i,k+\frac{1}{2}}^{n+1}$ from the impervious bottom to the free-surface. Specifically, equations (13)-(14) and (16) are first written in vector notation as

DOI: 10.1002/fld

$$\mathbf{A}_j^n \bar{\mathbf{u}}_j^{n+1} = \mathbf{G}_j^n - g\Delta t \frac{\eta_{r(j)}^{n+\theta} - \eta_{\ell(j)}^{n+\theta}}{\delta_j} \bar{\mathbf{a}}_j^n \tag{18}$$

$$\tilde{\mathbf{u}}_j^{n+1} = -\mathbf{K}_j^n \frac{\eta_{r(j)}^{n+1} - \eta_{\ell(j)}^{n+1}}{\delta_j} \tag{19}$$

$$V_i(\eta_i^{n+1}) = V_i(\eta_i^n) - \Delta t \sum_{j \in S_i} \sigma_{i,j} \left[\left(\bar{\mathbf{a}}^\top\right)_j^n \bar{\mathbf{u}}_j^{n+\theta} + \left(\tilde{\mathbf{a}}^\top\right)_j^n \tilde{\mathbf{u}}_j^{n+\theta} \right] \tag{20}$$

where $\mathbf{A}_j^n$, is a symmetric, positive definite, tridiagonal matrix that includes bottom friction and vertical viscosity terms; $\bar{\mathbf{u}}_j^{n+1}$ and $\tilde{\mathbf{u}}_j^{n+1}$ are vectors containing the unknown surface velocities $\bar{u}_{j,k}^{n+1}$ and the subsurface velocities $\tilde{u}_{j,k}^{n+1}$, respectively; $\bar{\mathbf{a}}_{j,k}^n$ and $\tilde{\mathbf{a}}_j^n$ are vectors whose entries are the vertical face areas $\bar{a}_{j,k}^n$ and $\tilde{a}_{j,k}^n$, respectively; and $\mathbf{G}_j^n$ is a vector containing the known explicit terms in Equation (13).

Formal substitution of $\bar{\mathbf{u}}_j^{n+1}$ and $\tilde{\mathbf{u}}_j^{n+1}$ from (18) and (19) into (20) yields the following discrete free-surface equation

$$V_i(\eta_i^{n+1}) - \theta\Delta t \sum_{j \in S_i} \left\{ \left[g\theta\Delta t \, \left(\bar{\mathbf{a}}^\top \mathbf{A}^{-1} \bar{\mathbf{a}}\right)_j^n + \left(\tilde{\mathbf{a}}^\top \mathbf{K}\right)_j^n \right] \frac{\eta_{\wp(i,j)}^{n+1} - \eta_i^{n+1}}{\delta_j} \right\} = b_i^n \tag{21}$$

where b_i^n is given by

$$b_i^n = V_i(\eta_i^n) - \Delta t \sum_{j \in S_i} \sigma_{i,j} \left[(1-\theta) \left(\bar{\mathbf{a}}^\top \mathbf{u} + \tilde{\mathbf{a}}^\top \tilde{\mathbf{u}}\right)_j^n + \theta \left(\bar{\mathbf{a}}^\top \mathbf{A}^{-1} \mathbf{G}\right)_j^n \right]$$

Equations (21) can be assembled into a sparse, *mildly nonlinear* system of N_p equations for η_i^{n+1}. This system has a symmetric, and at least positive semi-definite linear part. Thus, in absence of ceiling ($c \equiv \infty$), if the porosity function $\epsilon(x, y, z)$ is a non decreasing function of the vertical coordinate z for all $(x, y) \in \Omega$, then the mildly nonlinear system of Equations (21) can be efficiently solved to machine accuracy by a Newton type method with quadratic convergence rate [11, 18].

In general, however, the volume functions $V_i(\eta)$ are neither concave nor convex (see Figure 3). Consequently a direct application of the Newton method to system (21) may fail to converge unless the initial guess is sufficiently close to the unknown solution [13, 14, 19]. For this reason a nested Newton type method described in Reference [15] is better suited because fast convergence can

Prepared using fldauth.cls http://mc.manuscriptcentral.com/fluids DOI: 10.1002/fld

be assured under rather general assumptions on the soil properties and geometric details (see also [13, 14, 19, 20, 21]).

Once the new free-surface location has been determined, Equations (18) constitute a set of N_s *linear*, tridiagonal systems with at most N_z equations each. All these systems are independent from each other, symmetric and positive definite. Thus, they can be conveniently solved by a direct method to obtain the horizontal surface velocities $\bar{u}^{n+1}$. The discrete subsurface velocities $\tilde{u}^{n+1}$ are readily determined from Equations (19).

Finally, now that the new horizontal velocities have been computed throughout, the new vertical component of the velocity can be diagnostically determined from the discrete incompressibility condition (15). This equation, in fact, can be rearranged to yield the following recursive relation for the face averaged vertical velocities in each water column

$$\begin{aligned} w^{n+1}_{i,m-\frac{1}{2}} &= 0; \\ w^{n+1}_{i,k+\frac{1}{2}} &= \frac{a^n_{i,k-\frac{1}{2}} w^{n+1}_{i,k-\frac{1}{2}} - \sum_{j\in S_i} \sigma_{i,j} a^n_{j,k} u^{n+1}_{j,k}}{a^n_{i,k+\frac{1}{2}}}, \qquad k = m_i, m_i+1, \ldots, M^n_i - 1 \end{aligned} \tag{22}$$

In summary, assuming the knowledge of $\bar{u}^n$, $\tilde{u}^n$, w^n and η^n from the previous time level t_n, each time step is advanced by preliminarily determining the wet lengths λ^n from (8) and the wet areas $\bar{a}^n$, $\tilde{a}^n$ and a^n from (9), (10) and (12), respectively; then the mildly nonlinear system (21) is solved iteratively to obtain *simultaneously* the new water level η^{n+1} and the corresponding fluid volumes $V(\eta^{n+1})$; next, the new horizontal velocities $\bar{u}^{n+1}$ are obtained as solution of the N_s linear tridiagonal Systems (18); the discrete subsurface velocities $\tilde{u}^{n+1}$ are readily determined from Equation (19); and, finally, the new vertical velocities w^{n+1} are diagnostically determined from Equation (22).

6. HINTS AND REMARKS

It can be shown that the stability of the semi-implicit method (13)-(16) remains independent of the celerity, friction and vertical viscosity provided that $\frac{1}{2} \leq \theta \leq 1$ (see [9]). The stability does depend

DOI: 10.1002/fld

on the discretization of the advection and horizontal viscosity terms. In other words, when F is stable and $\frac{1}{2} \leq \theta \leq 1$, then the resulting discrete model (13)-(16) is also stable.

It should be noted that, the size and the structure of the mildly nonlinear system (21) is independent from the vertical resolution and from the prescribed subgrid details. Subgrid, and vertical resolution affect the assembly of Equation (21) and the number of equations for horizontal and vertical velocities. Moreover, since a major part of the computational effort is required to determine the free-surface elevation from Equations (21), a detailed subgrid data and a fine vertical resolution can be adopted with an acceptable increase of the corresponding computational effort.

On the other hand, if only one vertical layer is specified ($N_z = 1$), then equations (13)-(16) simplify to a consistent approximation for the coupled surface-subsurface model governed by the two-dimensional shallow water equations for the surface flow, and by the two-dimensional Boussinesq equations for the subsurface flow. A one-dimensional model with arbitrarily shaped cross sections is also obtained from the present formulation by further arranging the unstructured orthogonal grid in such a fashion that each polygon Ω_i has at the most 2 neighbors.

Additionally, if/where the soil level coincides with the impervious bottom ($s(x, y) = h(x, y)$), then only surface flow is allowed and can be simulated by the present method as a particular case. This case was reported in Reference [12]. Similarly, if/where the soil level coincides with the ceiling ($s(x, y) = -c(x, y)$), then only subsurface flow is allowed and can be simulated by the present method as another particular case (see [15]).

More importantly, when this method is applied to a complex flow region which includes extended shallow areas, deep and shallow tributaries, then each section of the region gets its own correct representation without any special treatment at the interfaces.

The proposed method, whose general formulation has been presented above in its simplest form, can be further modified in many ways to simulate a variety of specific free-surface problems. As an example, sources and/or sinks can be included by simply allowing a nonzero right hand side to the continuity Equations (6)-(7). Also, additional forces such as Coriolis or baroclinic pressure can be considered by including appropriate terms to the velocity Equations (1)-(2) and (4)-(5). This implies

DOI: 10.1002/fld

a reformulation of the term Fu_j^n in (13), hence a modified right hand side of System (21) will result. An additional advection diffusion equation may also be included to model the transport of scalar variables such as salinity, water temperature and/or pollutants.

7. NUMERICAL TESTS

The accuracy, the efficiency and the robustness of the proposed method for simulating surface flow problems within a subgrid environment has been already documented in the recent literature [11, 12, 13, 22, 23] and will not be duplicated here. Also, the applicability of this method to simulate saturated-unsaturated flows in confined-unconfined aquifers has been shown in [15, 18, 14, 19].

In this section the applicability the above method is briefly shown on a few illustrative test cases where the interaction of surface and subsurface flows plays an important role. Specifically, the first test case concerns a one-dimensional flow and water exchange between a tidal basin and an adjacent lagoon through an interposed sandy embankment. In a second test, the overland two-dimensional flow resulting from an intense and long lasting rainfall on a V-shaped catchment basin is simulated with and without soil absorbtion. Finally, a three-dimensional computation of a dam break flow illustrates the inundation of 'porous' building located along the flood plain.

The proposed method has been implemented in a single, general purpose computer code which includes options for scalar transport, for baroclinic and for non hydrostatic pressure. The specific momentum advection operator that is used for these test cases is an Eulerian-Lagrangian extension of the explicit conservative scheme discussed in References [17, 20]. Moreover, the bottom friction coefficient adopted in these specific tests is assumed to be $\gamma = g\frac{\sqrt{(u^*)^2+(v^*)^2}}{C_z^2}$, where C_z is the Chezy's bed roughness coefficient.

In every run the system of free-surface Equations (21) is solved to machine accuracy in order to obtain a precise mass conservation. In all tests the qualitative aspects of the computed results will be emphasized. All calculations have been performed on a laptop with an Intel i7 CPU having $2.80\,GHz$ clock frequency and $6\,GB$ of RAM.

DOI: 10.1002/fld

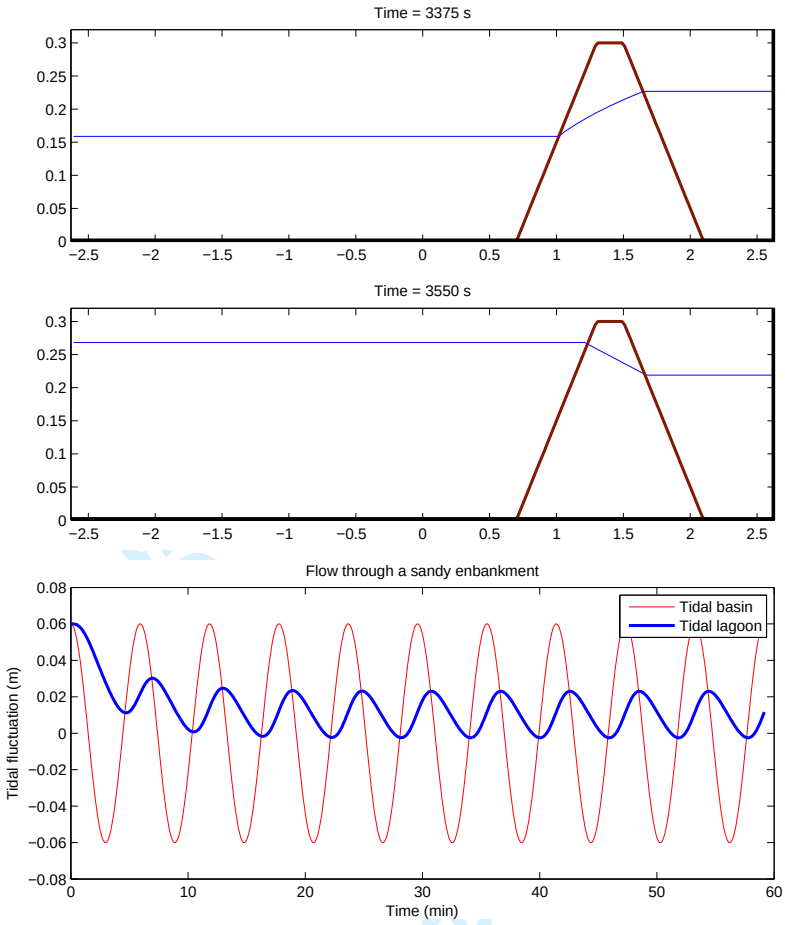

Figure 4. Low tide, high tide, and tidal fluctuation computed at both sides of the sandy embankment

7.1. *Flow in a tidal lagoon*

In this test the flow and water exchange between an idealized tidal basin and an adjacent lagoon is simulated. The tidal basin and the lagoon are separated by a trapezoidal sandy embankment characterized by a constant porosity $\epsilon = 0.3$ and hydraulic conductivity $\mathcal{K} = 0.01\, m/s$ (see Figure 4). For the surface flow the horizontal viscosity is neglected ($\nu^h = 0$) and the Chezy's bed roughness coefficient is taken to be $C_z = 50\, m/s$.

Observations and measurements of an experimental two-dimensional groundwater transport through the sand embankment between the wetland and the coastal area have been reported in Reference [24]). Here, for simplicity, only a (one-dimensional) longitudinal section of the model is considered.

Prepared using fldauth.cls http://mc.manuscriptcentral.com/fluids DOI: 10.1002/fld

The one-dimensional horizontal flow region $\Omega = [-2.64, 2.64]$ has a total length $L = 5.28\,m$. This region is covered with $N_p = 264$ uniform segments Ω_i of length $\lambda_j = \delta_j = 2\,cm$, and the implicitness parameter is set to $\theta = 0.6$. A constant depth is set to $h(x) = 0$; the trapezoidal sandy embankment is prescribed by specifying $s(x) = min\left[0, max\left(-0.33, \frac{1}{2}|x - 1.04| - 0.35\right)\right]$; and the ceiling is neglected ($c(x) = \infty$).

At the initial time $t_0 = 0$ the flow is at rest and the prescribed initial water level is set to $\eta(x, t_0) = 0.274\,m$ everywhere. Then a no flow boundary condition is prescribed at the right boundary ($u(\frac{L}{2}, t) = 0$), and a periodic (tidal) boundary condition on the free-surface elevation is prescribed at the left boundary as $\eta(-\frac{L}{2}, t) = 0.214 + a\,cos(2\pi t/T)$, where $T = 355\,s$ is the tidal period and $a = 0.06\,m$ is the tidal amplitude. The simulation is carried on for 10 tidal cycles with a time step size $\Delta t = 5\,s$. The elapsed computing time to complete the entire simulation is only $T_{cpu} = 6\,s$.

Figure 4 shows the water level at low and at high tide. This figure also shows the time series for the water level relative to the mean sea level in the tidal basin and in the lagoon, respectively. The water surface oscillation in the lagoon has a near 90^0 phase lag compared with the tidal oscillation, and the average water level in the lagoon is higher than that in the tidal basin. These results are in good agreement with the measurements, and with previously computed results [2, 4, 24, 25]).

7.2. Overland flow over a V-shaped catchment

In this test the overland flow resulting from an intense and long lasting rainfall is simulated and compared with and without soil absorbtion, see References [26, 27]. The spatial V-shaped domain includes an overland region, a channel and a subsurface region characterized by constant porosity $\epsilon = 0.1$ and hydraulic conductivity $\mathcal{K} = 5 \times 10^{-5} m/s$. For the surface flow the horizontal viscosity is neglected ($\nu^h = 0$) and the Chezy's bed roughness coefficient is taken to be $C_z = 10\,m/s$.

The flow domain Ω consists of a $1000\,m \times 1620\,m$ slope which includes a $1000\,m$ long channel of width $D = 20\,m$. The depth of the channel has a slope $s_c = 0.02$ and varies from $0\,m$ at the upstream end to $20\,m$ at the downstream end, whereas the surface slope is $s_s = 0.05$ in the

Prepared using fldauth.cls http://mc.manuscriptcentral.com/fluids DOI: 10.1002/fld

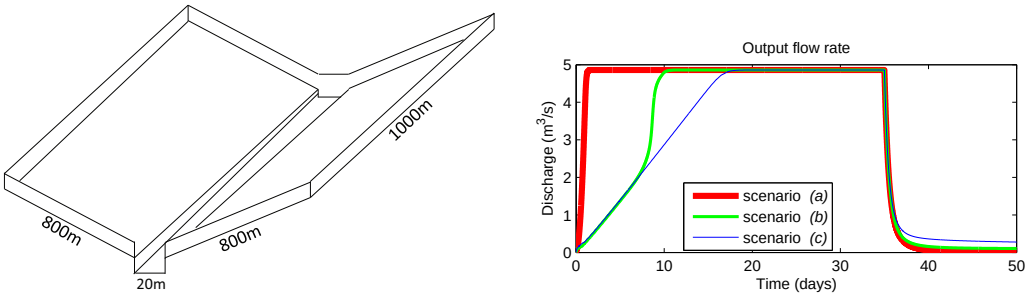

Figure 5. V-catchment and discharge at the channel outflow

transversal direction perpendicular to the channel. Thus, assuming that the origin is located at the center of Ω, the soil level is given by $s(x,y) = -0.05|x|$ for all $(x,y) \in \Omega$ and $|x| \geq 10\,m$; and $s(x,y) = 10 - 0.02y$ for all $(x,y) \in \Omega$ and $|x| < 10\,m$ (see Figure 5).

The flow region Ω is covered with a total of $N_p = 4\,050$ uniform squares Ω_i with $\lambda_j = \delta_j = 20\,m$, and the implicitness parameter is set to $\theta = 0.6$. At the initial time $t_0 = 0$ the fluid is at rest with a constant water level $\eta(x,y,t_0) = 0$ so that the surface water is confined within the channel. A no flow boundary condition is applied everywhere except at at the downstream end of the channel where the water level is maintained to be $\eta = 0\,m$ for all times $t > t_0$.

The flow is generated by a rainfall event with a high rainfall rate of $r = 3 \times 10^{-6} m/s$ which is applied everywhere in Ω for $35\,days$, with $zero$ rainfall for the subsequent $15\,days$ of recession [27, 28].

The simulation is carried on for $12\,000$ time steps with a time step size $\Delta t = 6\,min$ until the final time $T = 50\,days$ is reached. Figure 5 (right) shows the resulting outflow hydrograph corresponding to 3 different scenarios, namely (a) purely surface flow obtained by setting everywhere $h(x,y) = s(x,y)$, (b) coupled surface-subsurface flow that results from prescribing a $20\,m$ soil layer, i.,e., $h(x,y) = s(x,y) + 20$, and (c) flat impervious bottom given by prescribing $h(x,y) = 40\,m$ for all $(x,y) \in \Omega$.

As expected, the purely surface flow shows sharper rising and receding limbs; with a $20\,m$ soil layer the outflow hydrograph shows a rising limb occurring at a slower rate than for overland flow alone and gets steeper as the soil becomes saturated. This is more evident with a flat impervious

Prepared using fldauth.cls http://mc.manuscriptcentral.com/fluids DOI: 10.1002/fld

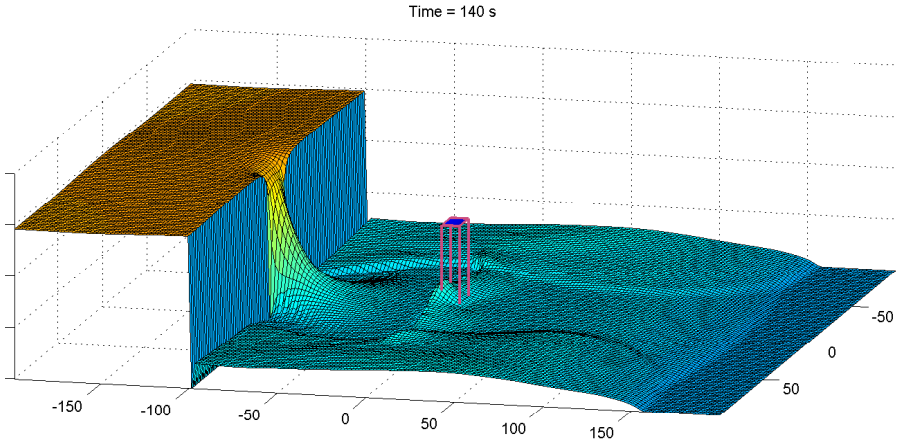

Figure 6. Three-dimensional dam break inundation

layer because in this case the subsurface region is larger permitting a larger water storage. The receding limb shows a distinct break between the overland runoff component and the baseflow component which continues for a longer period at a slower and more gradually declining rate. The elapsed computing times to complete the three simulations are $T_{cpu} = 128\,s$, $T_{cpu} = 139\,s$, and $T_{cpu} = 144\,s$, respectively.

7.3. Three-dimensional dam break inundation

In this last test the inundation of a flood plain after a dam break is simulated. The flow domain Ω is a rectangle of length $L = 400\,m$ and width $D = 200\,m$ partially occupied by a reservoir at the left-hand side. At the right-hand side of the reservoir a $20\,m$ wide gate, placed symmetrically along the center line in the longitudinal direction, connects the reservoir with the flood plain, which is open only at the right-hand side. Additionally, a square building of side $12\,m$ is centrally located in Ω (see Figure 6). This building is assumed as a porous material with a porosity $\epsilon = 0.8$ and hydraulic conductivity $\mathcal{K} = 50\,m/s$ [2]. For the surface flow the horizontal viscosity is neglected ($\nu^h = 0$), the vertical viscosity is set to $\nu^v = 10^{-3}\,m^2/s$, and the Chezy's bed roughness coefficient is taken to be $C_z = 50\,m/s$. Initially the water depth in the reservoir is $2\,m$ and the floodplain is dry.

Numerically, the horizontal domain Ω is covered with a uniform horizontal grid having grid size $\lambda_j = \delta_j = 2\,m$ and resulting in $N_p = 20\,000$ control volumes for each vertical layer. Additionally,

Prepared using fldauth.cls http://mc.manuscriptcentral.com/fluids DOI: 10.1002/fld

the vertical dimension of height $H = 2\,m$ is discretized with 20 vertical layers having uniform thickness $\Delta z_k = 0.1\,m$, and the implicitness parameter is set to $\theta = 1$. At the initial time $t_0 = 0$ the gate is instantaneously removed and the dry region, including the building, gets flooded.

This simulation is carried out for 800 time steps using a time step size $\Delta t = 0.25s$ until a final time $T = 200\,s$ is reached. The elapsed computing time to complete the entire simulation is $T_{cpu} = 456\,s$. Figure 6 shows the computed water levels at $t = 140\,s$. These results are in good agreement with the expectation and with previously computed results [2].

8. CONCLUSIONS

The governing differential equations for velocities are derived from the Navier-Stokes equations and from the Darcy's law under the assumption that the flow is prevalently horizontal so that the hydrostatic approximation is valid. A conservative form of the free-surface equation expresses the time rate of the water level in terms of both, the surface, and subsurface horizontal integral fluxes.

Numerically, an unstructured orthogonal grid, possibly including subgrid details, is chosen in such a fashion that entire flow domain is represented with the desired spatial resolution. Then an implicit finite difference approximation of the Darcy's laws provides a linear relationship between the horizontal subsurface velocities and the unknown water levels. Likewise, an appropriate semi-implicit finite difference approximation of the momentum equations provides a linear relationship between the horizontal surface velocities and the unknown water levels. A linear implicit finite volume approximation of the incompressibility condition relates the unknown horizontal velocities to the discrete vertical velocities in both, the surface and in the subsurface flow domain. Finally, the free-surface equation is approximated by a conservative semi-implicit method expressing the new water volumes in terms of the total horizontal fluxes over the entire water column.

From the computational point of view, a formal substitution of the unknown velocities into the discrete free-surface equation leads to a well posed mildly non linear system where the new free-surface elevations are the only unknowns. This reduced system can be solved iteratively and yields, *simultaneously*, the new free-surface location and the corresponding fluid volume on each water

Prepared using fldauth.cls http://mc.manuscriptcentral.com/fluids DOI: 10.1002/fld

column. Once the new free surface is known, the horizontal velocities are readily computed from the discrete velocity equations and, finally, the new vertical component of the velocity is recovered recursively from the discrete incompressibility condition.

The resulting method is extremely efficient, mass conservative, and the time step size is not restricted by a stability conditions dictated by surface wave speed, wall friction or vertical viscosity. Moreover, for any time step size the computed fluid volumes are assured to be everywhere nonnegative and wetting and drying for both, the surface and the subsurface flow regions, is naturally obtained at subgrid level. A few computational examples show the applicability of the proposed method to a variety of surface-subsurface flow problems.

REFERENCES

1. Bear J., Verruijt A. *Modeling Groundwater Flow and Pollution*, D. Reidel, Dordrecht, Holland, 1987.
2. Liang D, Falconer RA, Lin B. Coupling surface and subsurface flows in a depth averaged flood wave model. *Journal of Hydrology* 2007; **337**:147–158.
3. Spanoudaki K, Stamou AI, Nanou-Giannarou A. Development and verification of a 3-D integrated surface water–groundwater model. *Journal of Hydrology* 2009; **375**:410–427.
4. Kong J, Xin P, Song Z-y, Li L. A new model for coupling surface and subsurface water flows: With an application to a lagoon. *Journal of Hydrology* 2010; **390**:116–120.
5. Yuan L-R, Xin P, Kong J, Li L, Lockington D. A coupled model for simulating surface water and groundwater interactions in coastal wetlands. *Hydrological Processes* 2011; **25**:3533–3546.
6. Miglio E, Quarteroni A, Saleri F. Coupling of free surface and groundwater flows. *Computers & Fluids* 2003; **32**:73–83.
7. Casulli V. Semi-implicit finite difference methods for the two-dimensional shallow water equations. *Journal of Computational Physics* 1990; **86**:56–74.
8. Casulli V, Cheng RT. Semi-implicit finite difference methods for three-dimensional shallow water flow. *International Journal for Numerical Methods in Fluids*. 1992; **15**:629–648.
9. Casulli V, Cattani E. Stability, accuracy and efficiency of a semi-implicit method for three-dimensional shallow water flow. *Computers & Mathematics with Applications* 1994; **27**:99–112.
10. Casulli V, Walters RA. An unstructured grid, three-dimensional model based on the shallow water equations. *International Journal for Numerical Methods in Fluids* 2000; **32**:331–348.

11. Casulli V. A high-resolution wetting and drying algorithm for free-surface hydrodynamics. *International Journal for Numerical Methods in Fluids* 2009; **60**:391–408.
12. Casulli V, Stelling GS. Semi-implicit subgrid modelling of three-dimensional free-surface flows. *International Journal for Numerical Methods in Fluids* 2011; **67**:441–449.
13. Casulli V, Stelling GS. A semi-implicit numerical model for urban drainage systems. *International Journal for Numerical Methods in Fluids* 2013; **73**:600–614.
14. Brugnano L, Casulli V. Iterative solution of piecewise linear systems and applications to porous media. *SIAM Journal on Scientific Computing* 2009; **31**:1858–1873.
15. Casulli V, Zanolli P. Iterative solutions of mildly nonlinear systems. *Journal of Computational and Applied Mathematics* 2012; **236**:3937–3947.
16. Cordano E, Rigon R. A mass-conservative method for the integration of the two-dimensional groundwater (Boussinesq) equation. *Water Resources Research* 2013; **23**:1058–1078.
17. Stelling GS, Duynmeyer SPA. A staggered conservative scheme for every Froude number in rapidly varied shallow water flows. *International Journal for Numerical Methods in Fluids* 2003; **43**:1329–1354.
18. Brugnano L, Casulli V. Iterative solution of piecewise linear systems. *SIAM Journal on Scientific Computing* 2008; **30**:463–472.
19. Casulli V, Zanolli P. A nested Newton type algorithm for finite volume methods solving Richards' equation in mixed form. *SIAM Jour. on Scientific Computing* 2010; **32**:2255–2273.
20. Casulli V. A semi-implicit numerical method for the free surface Navier-Stokes equations. *International Journal for Numerical Methods in Fluids* 2014; **74**:605–622.
21. Dumbser M, Uwe I, Ioriatti M. An efficient semi-implicit finite volume method for axially symmetric compressible flows in compliant tubes. *Applied Numerical Mathematics* 2015; **89**:24–44.
22. Sehili A, Lang G, and Lippert C. High-resolution subgrid models: a background, grid generation, and implementation. *Ocean Dynamics* 2014; **64**:519–535.
23. Wang HV, Loftis JD, Liu Z, Forrest D, Zhang J. The Storm Surge and Sub-Grid Inundation Modeling in New York City during Hurricane Sandy. *Journal of Marine Science and Engineering* 2014; **2**:226–246.
24. Ebrahimi K, Falconer RA, Lin B. Flow and solute fluxes in integrated wetland and coastal systems. *Environmental Modelling & Software* 2007; **22**:1337–1348.
25. Yuan B, Yuan D, Sun J, Tao J. A finite volume model for coupling surface and subsurface flows. *Procedia Engineering* 2012; **31**:62–67.
26. Di Giammarco P, Todini E, Lamberti P. A conservative finite elements approach to overland flow: the control volume finite element formulation. *Journal of Hydrology* 1996; **175**:267–291.
27. Panday S, Huyakorn PS. A fully coupled physically-based spatially-distributed model for evaluating surface/subsurface flow. *Advances in Water Resources* 2004; **27**:361–382.
28. Sulis M, Meyerhoff SB, Paniconi C, Maxwell RM, Putti M, Kollet SJ. A comparison of two physics-based numerical models for simulating surface watergroundwater interactions. *Advances in Water Resources* 2010;

33:456–467.

DOI: 10.1002/fld